ADVANCED MATERIALS INTERFACES
www.advmatinterfaces.de

Interrogating the Effect of Assay Media on the Rate of Virus Inactivation of High-Touch Copper Surfaces: A Materials Science Approach

Carol F. Glover, Tsuyoshi Miyake, Victor Wallemacq, Jamie D. Harris, John Emery, Daniel A. Engel, Stephen J. McDonnell, and John R. Scully*

Contamination of high-touch surfaces with infected droplets of bodily secretions is a known route of virus transmission. Copper surfaces have been reported to inactivate human coronaviruses after several minutes, via the release of Cu cations. Utilization of copper alloys for high-touch surfaces can be a pivotal preemptive strategy for preventing the next pandemic. Understanding the true efficacy by which copper, and copper alloys, inactivate the virus under realistic conditions is essential for tuning intrinsic alloy features such as composition, grain orientation, and surface attributes, to optimize for antiviral function. However, virus inactivation measurements depend on the presence of an assay media (AM) solution as a carrier for the virus, and its effects on the surface properties of pure copper that regulate oxidative copper release are previously unknown. Herein, these properties and the influence of AM on the efficacy of virus inactivation occurring on the surface of pure copper are investigated. The process is uncovered by which a five-fold decrease in virus half-life is observed in simulated real-life conditions, relative to exposure to traditional AM. The investigation highlights the notion that virus inactivation on copper surfaces may be significantly more effective than previously thought.

1. Introduction

Human coronaviruses (such as SARS-CoV-1, SARS-CoV-2, OC43, and 229E) have been shown to remain infectious for up to five days on common non-biocidal surfaces, including stainless steel, glass, and ceramic tile.[1,2] While the most effective form of virus-transmission is through inhalation of air, carrying aerosol particles containing infectious virus,[3] projected by coughing and sneezing, transfer through touching contaminated surfaces still poses a risk.[4] Following hand-contact, virus particles may be transferred to the facial mucosa of a novel host upon touching the eyes, nose, and mouth.[4]

High-touch surfaces, such as door-handles and hand-rails, are prone to continuous recontamination.[5,6] As such, design of materials for high-touch surfaces that can inactivate viruses over short time-scales, is a high priority for materials scientists.[7–11] Copper and copper alloys have been demonstrated to possess excellent antiviral properties, via the release of soluble copper cations (such as Cu^{1+}) into the local environment, through an electrochemical corrosion process.[12–16] Their utilization of high-touch surfaces could be a pivotal preemptive strategy for preventing the next pandemic.[17–19] However, the efficacy and rate with which cations released from a copper surface can inactivate the virus has become a source of contention, where investigators report inactivation times ranging from the order of minutes, to several hours.[1,20,21] Doremalan et al. demonstrated a time of 4 h for SARS-CoV-2 to be inactivated on a copper surface,[1] and Robinson et al. demonstrated a time of 5 h for 99% inactivation of SARS-CoV-2 on a novel additively manufactured Copper-Tungsten-Silver alloy.[21] In stark contrast, Bryant et al. reported an inactivation time of one minute, citing the cell culture medium as a key reason for the disparity of results.[20] Bryant speculates that the L-glutamine culture medium used by Doremalan et al. will result in partial surface passivation as a result of $Cu(OH)_2$ precipitates, inhibiting copper cation release, resulting in a slower inactivation time.[20] Bryant states that GlutaMAX-1-fed viral cultures, used in their own study, would not passivate the copper.[20] However, no evidence has been provided to support the presence of $Cu(OH)_2$.

Measuring the true efficacy by which the virus is inactivated is essential to inform the tuning of copper alloys to the desired composition, and other metallurgical details such as phases and grain orientation, all adjustable for optimizing for a critical balance between corrosion, oxide formation,

C. F. Glover, V. Wallemacq, J. Emery, S. J. McDonnell, J. R. Scully
Department of Materials Science and Engineering
University of Virginia
395 McCormick Road, P.O. Box 400745, Charlottesville, VA 22904, USA
E-mail: cfg3p@virginia.edu
T. Miyake, D. A. Engel
Department of Microbiology, Immunology, and Cancer Biology
University of Virginia
Pinn Hall, 7224, P.O. Box 800734, Charlottesville, VA 22904, USA
J. D. Harris
Department of Engineering Systems and Environment
University of Virginia
151 Engineer's Way, P.O. Box 400747, Charlottesville, VA 22904, USA
The ORCID identification number(s) for the author(s) of this article can be found under https://doi.org/10.1002/admi.202200390.

DOI: 10.1002/admi.202200390

and ion release. Corrosion rates must be sufficient to release enough copper cations for desired antiviral function, while simultaneously suppressing undesirable tarnish-forming oxides (to sustain acceptable aesthetics, important for perceived cleanliness and hygiene in public spaces) or passivating oxides, which prevent the continued release of cations necessary for virus inactivation. The assay solutions, used as the medium through which the virus is exposed to the surface of interest in laboratory experiments, contain species that render a local environment that differs greatly from the bodily secretions present in real-life (such as perspiration or saliva). The local environment to which the copper surface is exposed dictates the composition, stability, and thickness of surface oxides, which in-turn regulates the amount of soluble copper cations released into solution, and thus, their availability for virus inactivation.[22,23] Modifications to the local environment can result in an enhancement, or inhibition, of cation release as mentioned briefly by Bryant.[20]

This calls into question whether virus inactivation tests performed in traditional assay media (AM) reliably represent the virus inactivation-rate that occurs in a real-life environment. Here, we investigate the inactivation-rate of human betacoronavirus OC43 (a close representation of SARS-CoV-2 used for experimental purposes)[24] on pure copper surfaces, using solutions made up of various compositions of: 1) a traditional AM, and 2) artificial perspiration (AP), where the latter represents the most common bodily secretion found on high-touch surfaces.[25] Tables S1 and S2, Supporting Information, presented in the Supporting Information, give details of the composition of AP and AM. In a traditional virus inactivation test, 100% AM is used as the virus carrier, however, it is possible to conduct such tests using other solutions. It should be noted that this is most practical when at least 10% AM is present. While tests in 100% AP may appear to be the obvious replication of the real-world environment, the AM is an essential carrier solution for the virus and full omission from the experiment makes data collection extremely difficult.

Herein, we discuss the mechanism through which the virus inactivation-rate on a 99.95 wt.% commercially pure (CP) copper surface is affected by the composition of the test media. We identify the optimum composition of a hybrid AP:AM solution that can enable accurate virus inactivation testing. All experiments were conducted in a range of solution compositions that comprised the following amounts of AP: 100%, 90%, 80% 60%, and 0% (with the exception of the virus inactivation tests, where the use of 100% AP was found to be highly impractical), with the balance being AM. This will enable extrapolation to 100% AP behavior in the virus inactivation tests. Electrochemical cyclic voltammetry (CV) experiments were utilized to quantify the oxidation of copper to form Cu(I) cation species (expressed as an anodic charge coupled with the moles of copper oxidized through Faraday's Law) through electrochemical oxidation of pure copper, after a period of immersion in the various solution compositions. Any solid-state corrosion products, that is, copper oxides, that formed on the surfaces of the copper during such immersions were also characterized using X-ray photoelectron spectroscopy (XPS), combined with electrochemical coulometric reduction (CR) experiments.[7,9]

2. Results

2.1. Inactivation-Rate of Betacoronavirus (OC43) in Various Media

The inactivation-rate of beta-coronavirus (OC43), was determined on CP copper surfaces, and on pure plastic control surfaces, in the various AM:AP solution component ratios. The data are presented in **Figure 1**a, and a summary of the virus half-life as a function of %AP content is presented in Figure 1b. A virus inactivation half-life of approximately 92 min was recorded for tests conducted in 100% AM, and the initial inactivation rate was found to be extremely slow in the first 60 min. In stark contrast, the virus inactivation half-life was found to be approximately 17 min for tests conducted in the solution containing 90% AP. The data show that the virus inactivation half-life increases progressively with increasing AM content (Figure 1b). For all test solution compositions regardless of AP:AM content, no virus inactivation was observed on the plastic control surfaces over an exposure period of 160 min. The data presented in Figure 1a enabled the selection of an immersion time for interrogation and analysis using electrochemical experiments and XPS to study CP copper surface reactivity and film-forming qualities after pre-exposures to the same solutions used for the virus inactivation tests. 20 min was selected as a highly representative pre-exposure immersion time, given the spread observed in the % of virus inactivation data across the range of solution compositions at this time (Figure 1a).

2.2. Electrochemical Oxidation of Pure Copper Following Exposure to Various Media

CV was employed to quantify the oxidation of CP copper to form Cu(I) cation species, following 20-min full-immersion pre-exposures to solutions at each AM: AP composition. Experiments were conducted in clean, Cu ion-free, deaerated borate buffer solution at pH 8.4 (i.e., where copper oxide are stable), such that only the solid Cu products were sampled. Representative voltammograms, selected from the third CV cycle, are presented in **Figure 2**a.

Copper oxidation was quantified by calculation of the charge associated with the oxidation peak that represents Cu(0) → Cu(I), as labeled in Figure 2c. On inspection of the recorded peaks, pre-exposures to 100% AP and 90% AP were found to produce a significantly larger Cu(0) → Cu(I) oxidation peak, relative to the experiments carried out in the other solution compositions. For clarity, the y-axis has been re-scaled to show the lower-intensity peaks and presented in Figure 2b. In each case, the charge associated with the Cu(0) → Cu(I) peak was calculated by dividing the applied potential-current density (E-I) peak area by the scan rate. A summary of the calculated charge, and the % of surviving virus after 20 min of exposure (extracted from Figure 1a), is presented in Figure 2d as a function of % AP in the exposure solution. Relative to the 100% AP pre-exposure, the measured charge associated with the Cu(0) → Cu(I) peak was found to be reduced by approximately 85%, 93%, and 87% after immersion in 0%, 60%, and 80% AP, respectively. In contrast, only a 5% reduction in charge was observed for pure copper samples pre-exposed to the 90% AP solution.

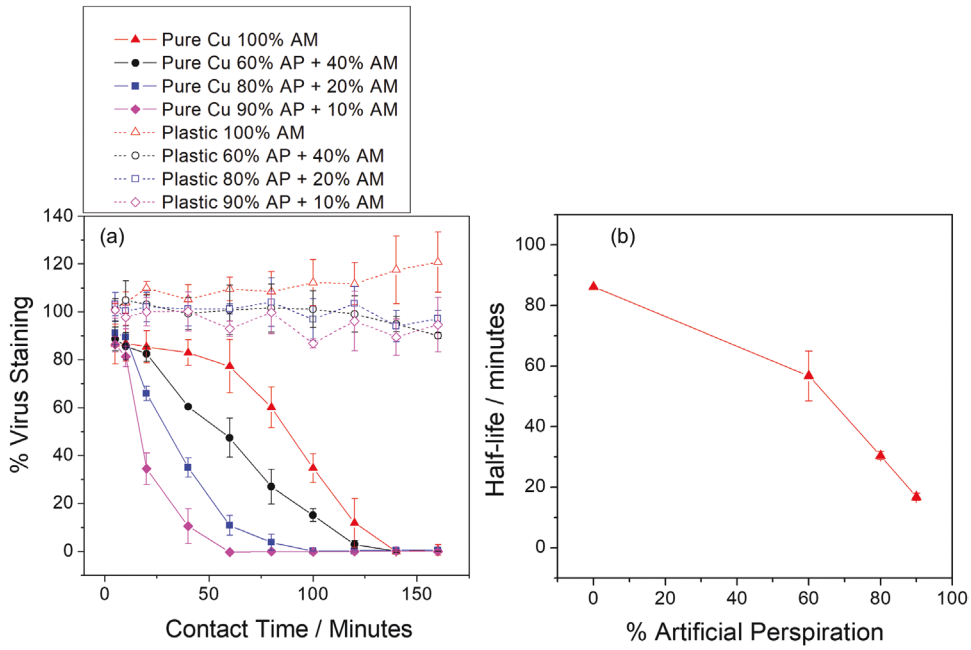

Figure 1. a) % Virus staining versus time for OC43 on pure Cu and plastic surfaces in solutions of various AM:AP composition ratios. b) Virus half-life as a function of AP content. Data are presented in terms of mean values ± standard deviation, where n = 3. For Figure 1(a) *p*-values between plastic and pure Copper were calculated using two-factor with the ANOVA statistical method with replication, for all time points $p < 0.01$. The *p*-values for pure Copper samples were calculated using one-factor ANOVA and, between 20 and 100 min, $p < 0.01$. For Figure 1(b) the *p*-value was calculated using one-factor ANOVA, where $p < 0.01$ ($p = 5.73 \times 10^{-7}$).

2.3. Characterization of Pure Copper Surface Phases Following Exposure to Various Media

XPS and electrochemical CR experiments were also utilized to characterize the surfaces of CP copper after 20-min full-immersion pre-exposures to solutions at each AM:AP composition. **Figure 3** shows XPS spectra measured on CP copper after pre-exposures to 100% AM and 100% AP. Considering the Cu $2p^{3/2}$ core level, the integrated intensity of the 100% AP specimen is almost entirely ascribed to Cu(I), accounting for 98%, with only 2% of Cu(0) (position linked to the less surface sensitive Cu 3p core level). Conversely, the integrated intensity of the specimen pre-exposed to 100% AM is dominated by 52% Cu(II), with only 44% Cu(I). The same trend is observed in the Cu LMM core level, with the integrated intensity of Cu(I) decreasing progressively between pre-exposure to 100% AP and 100% AM. An example of how the deconvolution of the metal and oxide peaks in the Cu LMM core level was performed is given in Figure S1, Supporting Information. Finally, the O 1s spectra corroborate the trend in Cu(I) oxide, where this is most evident in the specimen pre-exposed to 100% AP.

Comparing the copper core levels for the specimens pre-exposed to 100% AP and 100% AM, along with intermediary solution compositions (shown in Figures S4–S6, Supporting Information), a trend in the oxide states is evident. Oxide thickness calculations made using the presented XPS data are included in Section S1.1, Supporting Information, "Oxide Thickness Calculations". Specimens pre-exposed to 100% AP are dominated by Cu(I) with little to no Cu(II), and exhibit a thicker total oxide. Conversely, samples exposed to 100% AM feature a majority of Cu(II) and comparatively more of a Cu(0) integrated intensity (Figure 3), with a thinner total oxide (Figure 5b). A comparison of the Cu 2p spectra of the pure copper samples exposed to 100% AM and 100% AP is shown in Figure S2, Supporting Information.

An electrochemical CR technique was employed to further characterize CP copper after 20-min pre-exposures to solutions of each AP:AM composition. The technique has been used in multiple electrochemical investigations and provides information on the oxide composition and thickness (e.g., amount per unit area) via the establishment of reduction plateau's that can be assigned to a specific oxide species.[26–33] Data are presented in **Figure 4**a, where the potential (V vs SCE), resulting from cathodic galvanostatic holds at $-20\ \mu Acm^{-2}$, is plotted as a function of time. Four distinct plateau regions can be observed in all experiments where AM was present in the pre-exposure (labeled 1, 2, 3, and 4 in Figure 4).

The plateau at position 4, observed in all cases, is a result of the hydrogen evolution reaction (HER). Despite the presence of chlorides in both AP and AM (as listed in Tables S1 and S2, Supporting Information), chlorides were not detected by XPS on any sample containing AM. A low level (<3.2%) of chloride was detected on the specimen exposed to 100% AP. As such, none of the observed plateaus can be attributed to Cu—Cl compounds in the reduction test. The plateau at position 1 can be found at approximately –0.29 V versus SCE and was not observed in the experiment carried out with a pre-exposure to 100% AP. Given the limited detection of Cu(II) by XPS for this exposure condition, and the absence of a plateau at –0.29 V

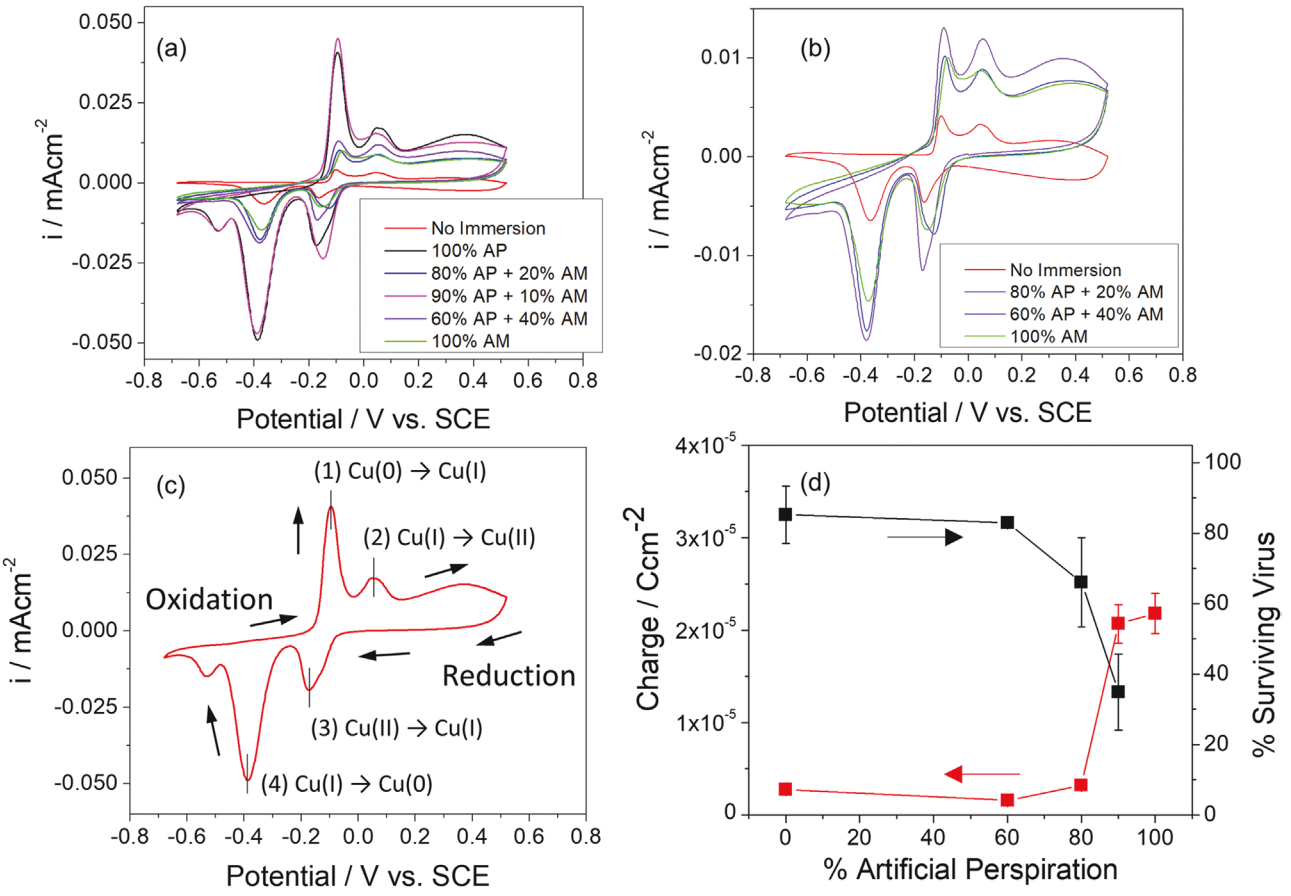

Figure 2. Cyclic voltammograms conducted on Pure Cu in deaerated borate buffer solution (pH 6.5), where the third cycle is given. Samples were first held for 20 min in various media and scan rate of 10 mV sec^{-1} was used. a) Data after immersion in all solutions, b) data after no immersion, 100% AM and 80% AP + 20% AM immersion, c) scan direction and the oxidation/reduction peak, and d) a plot showing the charge associated with the Cu(0) → Cu(I) oxidation peak and the % surviving virus as a function of AP content.

versus SCE (position 1), it seems reasonable to speculate that this plateau can be attributed to the reduction of CuO, via.

$$2CuO + H_2O + 2e^- \rightarrow Cu_2O + 2OH^- \quad \text{Reaction (1)}$$

$$E_{1/2} = 0.670 - 0.059pH\,(\text{V vs SHE}) \quad (1)$$

This was substantiated by XPS, where CP copper specimens pre-exposed to a solution of 40% AM: 60% AP were characterized following a CR hold that was terminated immediately after the first reduction plateau at position 1. Data are given in Figures S7–S10, Supporting Information. The same conclusion was drawn in previous investigations employing CR in comparable conditions.[32,33] Employing Equation (1), the data infers that the reduction of CuO occurs at a potential of –0.233 V versus SCE relative to the equilibrium potential for this reaction.

The plateaus labeled 2 and 3 in Figure 4a occur within the following potential ranges: (2) –0.39 V versus SCE to –0.51 V versus SCE and, (3) –0.57 V versus SCE to –0.69 V versus SCE. Various authors have demonstrated the presence of two such reduction plateaus, measured on pure copper, using CR holds[30,31] and linear sweep voltammetry (LSV),[28,29] and both authors attributed these potential plateaus to Cu_2O. This was verified using infrared reflection absorption spectroscopy (IRAS),[31] UV-visible NIR,[28] and XPS.[27] Persson et al. assigned the plateau at position 2 (i.e., at a more positive potential, relating to the more reducible species) to a Cu_2O precursor of Cu_xO, with the same crystallographic structure but containing mixed-valence states, where interstitial metallic Cu is present in the Cu(I) oxide phase.[31] Nonetheless, plateaus 2 and 3 can be attributed to the reduction of Cu_2O via,

$$Cu_2O + H_2O + 2e^- \rightarrow 2Cu + 2OH \quad \text{Reaction (2)}$$

$$E_{1/2} = 0.460 - 0.059pH\,(\text{V vs SHE}) \quad (2)$$

Employing Equation (2) gives potentials of approximately –0.144 V versus SCE and –0.294 V versus SCE relative to the equilibrium potential for this reaction for plateau 2 and plateau 3, respectively. It should be noted that a percentage of the Cu_2O reduced at position 2 will be as a result of the reduction of CuO at position 1, as per Reaction (1).

Figure 5a summarizes calculations made from Figures 3 and 4 where the oxide ratio of Cu(I):Cu(II) is given, as determined from the XPS Cu LMM core level fits (Figure 3) and

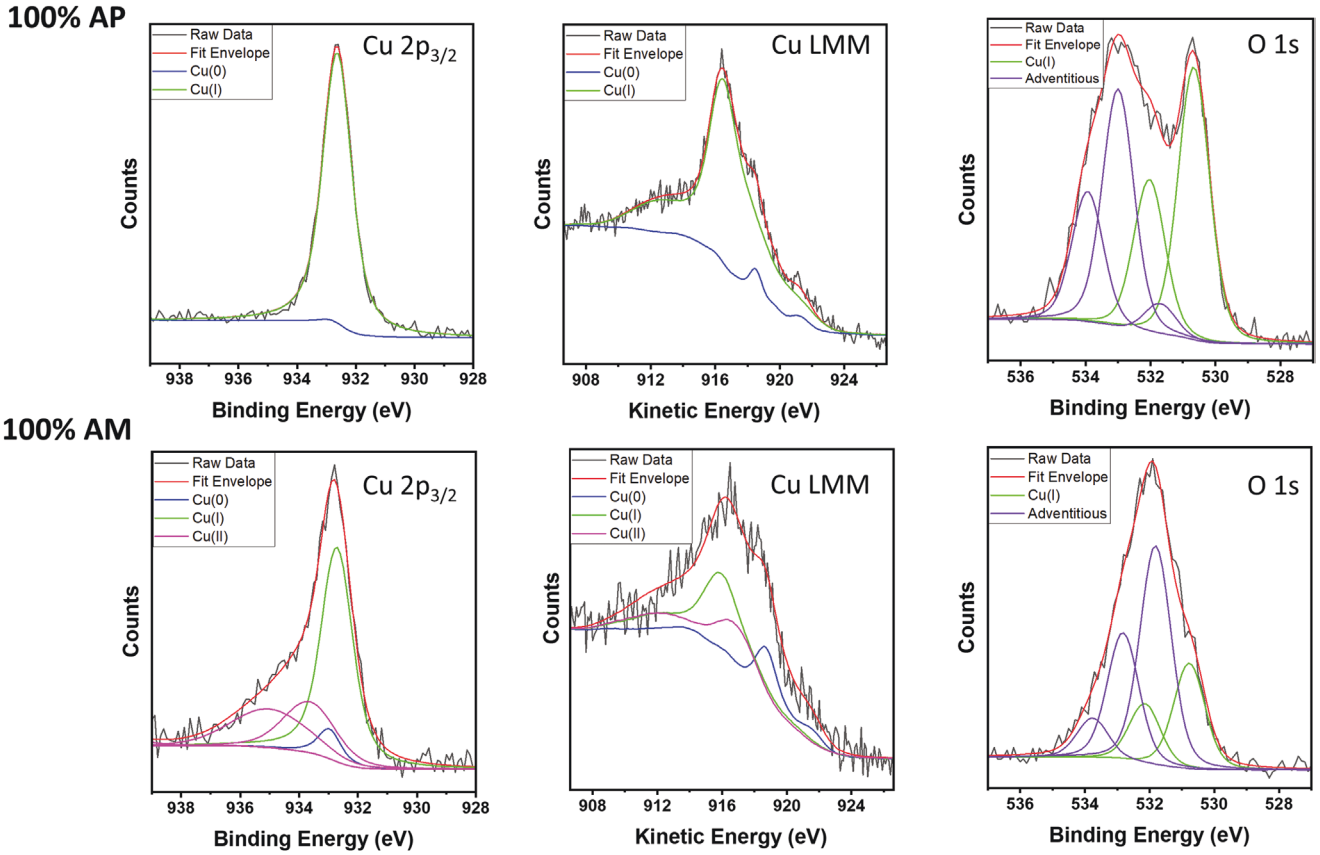

Figure 3. XPS Spectra measured on pure Cu after immersions in 100% AM and 100% AP.

from the CR data (Figure 4). The summary plots given in Figure S3, Supporting Information, provide additional information regarding the ratio of Cu(0):Cu(I):Cu(II) as measured via XPS from the Cu 2p core level (Figure S2(a), Supporting Information, and the Cu LMM core level (Figure S3(b), Supporting Information). Furthermore, Figure 5b compares the trends in total oxide thickness for each solution composition, as calculated separately from XPS and CR data. Details regarding the methods used to calculate oxide thickness are given in Section 5.2 and Section S1.1, Supporting Information, for CR experiments and XPS measurements, respectively. The data are in qualitative agreement that a trend of increasing Cu(I):Cu(II) oxide ratio (Figure 5a) and oxide thickness (Figure 5b) is observed with increasing AP content. A discussion of the systematic errors in these measurements that reduce accuracy more than precision is included in the SI.

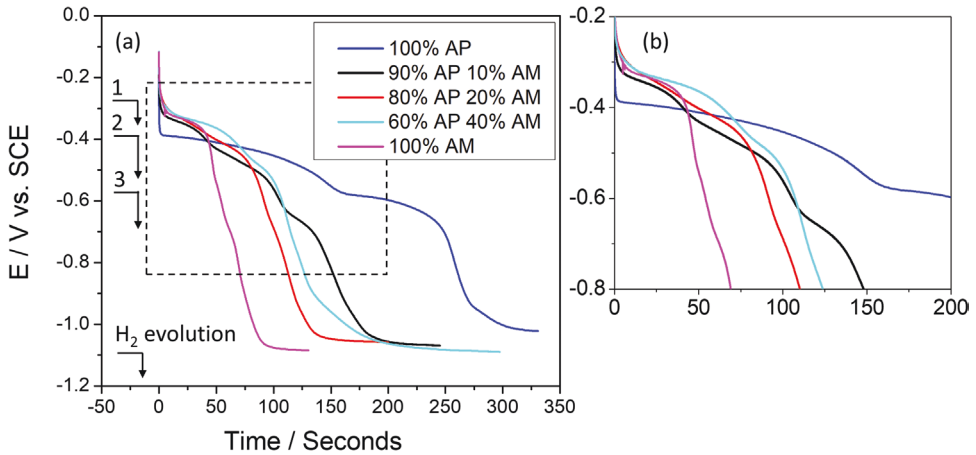

Figure 4. CR data measured in deaerated borate buffer solution (pH 8.4) on pure Cu after 20-min pre-exposures to solutions of various AM:AP composition ratios.

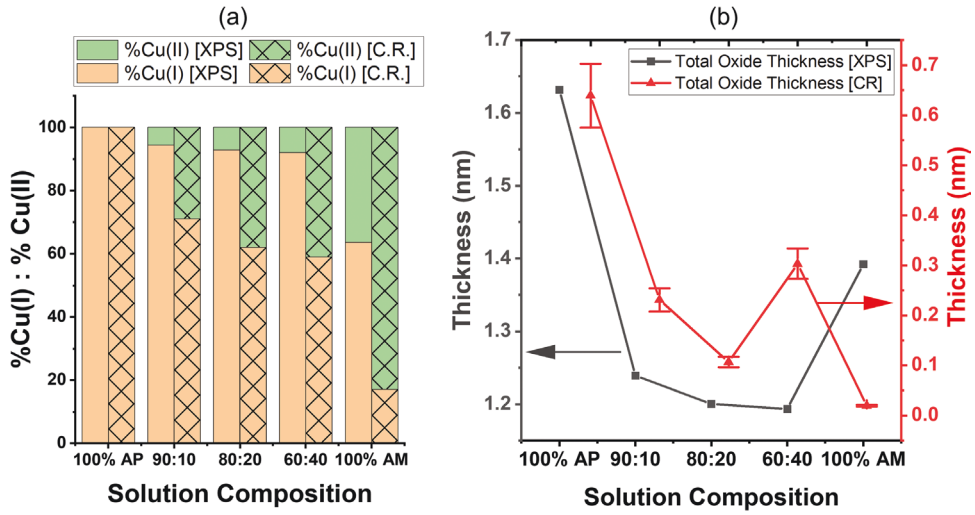

Figure 5. a) XPS Cu2p Spectra measured on pure Cu after immersions in 100% AM and 100% AP. b) Summary of total oxide thickness and ratio of Cu(i):Cu(ii) as measured using XPS and electrochemical CR data.

It is important to discuss the complete fate of copper in the alloy, at the surface in solid compound or as dissolved species in solution. Next, we turn our attention to the solution phase focusing on dissolving copper whether free ions or chelated.

2.4. Release of Cu Cations into Solution

It is of interest to quantify the copper released in a solution regulated by chemical and electrochemical processes. Inactivation is due to free Cu ions.[2] The total amount of Cu (in ppb) in AP and AM solutions following 20-min and, separately, 1-h immersions of CP copper was measured using graphite furnace atomic absorption spectrometry (GFAAS). The data is presented in **Figure 6** After 20 min, it can be observed that 33% more total copper was present in the AM solution, when compared to the AP solution. In contrast, after an immersion period of 1 h, 73% more Cu was measured in the AM solution, relative to the AP solution. Furthermore, an increase of only 15% Cu was measured in AP solution after 1 h of immersion relative to the amount of Cu measured after 20-min immersion. An increase of 66% Cu was measured in AM solution after 1 h, relative to the 20-min immersion). It should be noted that the GFAAS technique is not able to distinguish between oxidation states, and the total Cu in solution, including any chelated Cu, is captured in the measurement.[34] Since, free copper is antimicrobial, chelating in AM and AP must also be accounted for.

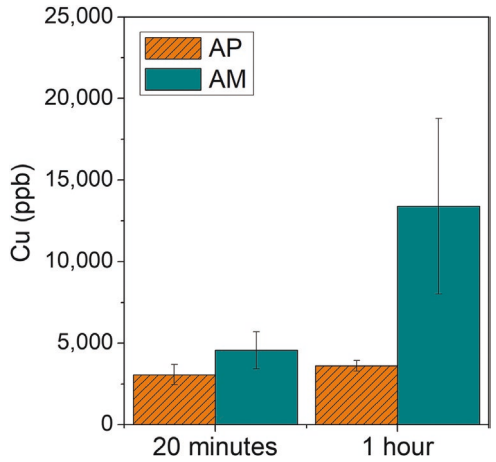

Figure 6. Bar chart showing the amount of Cu measured (ppb) in AM and AP solutions after the immersion of CP Cu for 20 min and 1 h, measured using GFAAS.

3. Discussion

The study presented herein demonstrates that exposure of 99.95 wt.% CP copper to a traditional virus inactivation AM test solution significantly inhibits the inactivation of the betacoronavirus (OC43) (Figure 1a), when compared to exposures to the solution containing AP solution. AP is representative of one of the most common bodily secretions found on high-touch surfaces.[25] We demonstrate that the systematic increase of the AM:AP ratio in the virus inactivation test solution progressively prolongs the half-life of the betacoronavirus (OC43) (Figure 1b). An increase in the virus inactivation half-life by a factor of 5 was observed when testing in 100% AM, when compared with tests conducted in 10% AM: 90% AP solution. A result of this nature is consistent with the virus inactivation test solution having a significant effect on one or more of the following factors: 1) the fate of oxidized species, that is, soluble cation release versus insoluble oxide formation, 2) the composition and thickness of surface oxides, 3) the rate of soluble cation-release into solution, 4) the oxidation state of soluble Cu cations released into solution (i.e., Cu(I) or Cu(II)), and 5) the availability of soluble cations released into solution, that is, chelating of Cu cations by species present in the solution, preventing their interaction with the virus, in contrast to the presence of free Cu(I) or Cu(II).

In assessment of the above factors, and the electrochemical, mass spectrometry, and surface characterization results

presented here, we can form a hypothesis regarding the mechanism by which the virus inactivation test solution affects the test itself. First, graphite furnace atomic absorption spectroscopy (GFAAS) measurements (shown in Figure 6 demonstrated that significantly more Cu cations were present in AM solution, relative to AP solution, after 20 and 60-min immersion times (33% and 73%, respectively). The expectation based on the relationship between free copper ion concentration is that larger concentrations inactivate at a higher rate.[2] Hence, this result strongly suggests that Cu chelating occurs in the AM solution, given the disparity in virus inactivation efficacy between 100% AM and 10% AM: 90% AP solution after 1 h of solution exposure (Figure 1), despite an approximately four-fold increase in soluble Cu release (Figure 2) in 100% AM. As such, chelated Cu cations would not be available for virus inactivation, as demonstrated in the schematic diagram given in **Figure 7**a. Chelators are typically organic compounds such as amino acids,[35–37] which make up a large portion of Dulbecco's modified eagle medium (DMEM 11965) which, in turn, makes up 97% of the total AM solution. The individual components of DMEM 11965 are listed in Table S2, and the amino acids listed can be identified as Cu chelators.[35] As such, it seems that exposure to the CP copper surface for an extended time period is required, such that the concentration of soluble Cu cations released is in excess of the rate of Cu chelation by the AM solution.

The electrochemical and XPS surface analysis data presented herein can provide insight into the mechanism through which large differences in soluble Cu release occur between AM and AP solutions. First, it should be recognized that copper oxidation results in both copper ions in solution and in solid corrosion products. The corrosion products can regulate the remaining copper release.

We have demonstrated using XPS and electrochemical CR (Figure 5) that pre-exposure of CP copper to test solutions containing any amount of AM, produces a different surface oxide composition than a pre-exposure to 100% AP solution. Increasing levels of AM content in the test solution resulted in an increasing fraction of Cu(II) oxide and, hence, the ratio of Cu(I):Cu(II) is found to decrease with increasing AM content (Figure 5a). We have demonstrated that Cu_2O was the dominant oxide resulting from a pre-exposure to 100% AP, while CuO was the dominant oxide resulting from pre-exposure to 100% AM (Figure 5). The solubility products (K_{sp}) of Cu_2O and CuO have been found to be 2.0×10^{-15} and 5.6×10^{-20},[38] respectively. This suggests that the CuO is 5 orders of magnitude less soluble and would be expected to provide a more chemically stable surface phase relative to Cu_2O. However, several additional factors contribute to electrochemical based copper release, for instance, the increased thickness of the oxide layer formed after pre-exposures to AP (Figure 5b) may provide a greater impediment to Cu ion release in the short

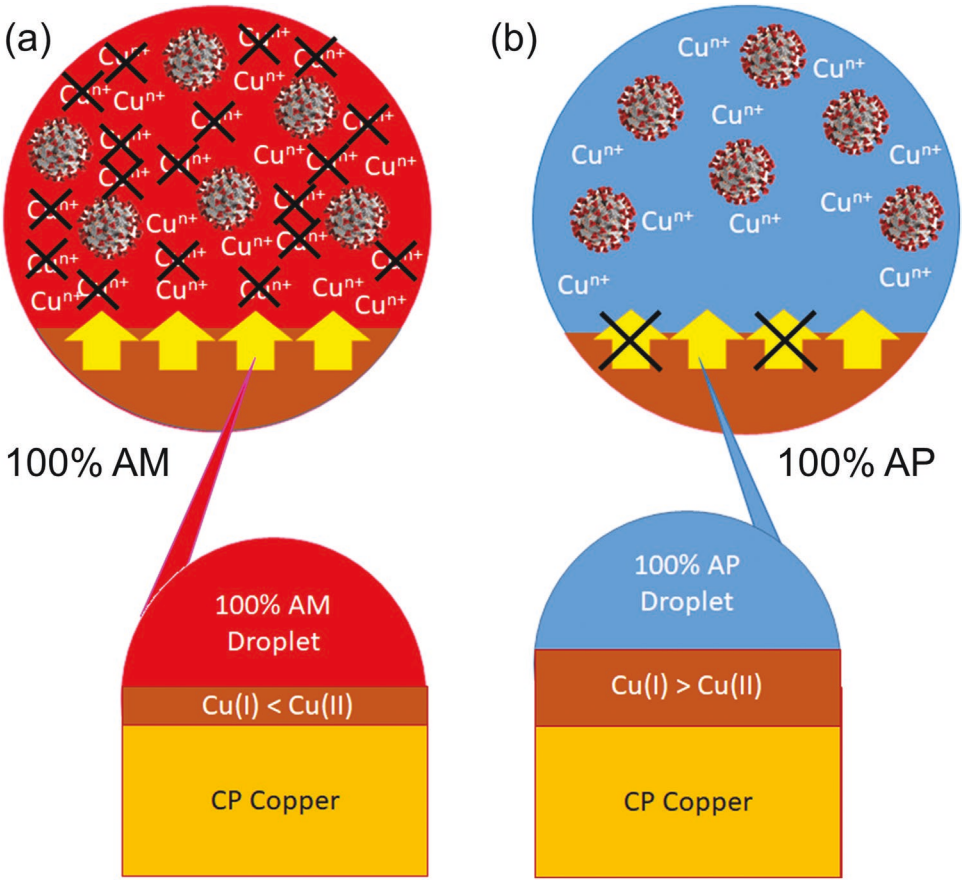

Figure 7. Schematic diagram showing the effects of virus inactivation test solution on the oxide and composition and thickness and the effect on Copper cation release for a) 100% AM, where the crosses represent chelated Cu^{n+} cations, and b) 100% AP where the crosses represent the limited cation release due to the oxide.

term even though it is more soluble, preventing or slowing electrochemical reactions occurring at the interface but requiring a potential field across the product film. As such, the total concentration of soluble Cu cations released is a complex function of all these features. The free copper available for virus inactivation could be suppressed by chelators. This proposed mechanism is represented in the schematic diagram given in Figure 7b.

It should be noted that several processes affecting virus inactivation may be occurring simultaneously, where the oxidation state of soluble Cu cations released into solution (i.e., Cu(I) or Cu(II)) may differ for CP copper exposed to AP or AM solutions. The oxidation state of the released soluble Cu species is important because Cu(I) has been shown to have greater efficacy for virus inactivation than Cu(II).[15] This is due to the role of Cu(I) in the occurrence of Fenton reactions that produce reactive oxygen species via:

$$Cu^{1+} + H_2O_2 \rightarrow Cu^{2+} + OH^- + OH^{\bullet} \quad \text{Reaction (3)}$$

Warnes et al. demonstrated that virus activation is primarily due to the direct action of Cu ions, but that some contribution from superoxide and hydroxyl radicals occurs.[2] In the absence of hydrogen peroxide in the contact solution, as is the case herein, Fujimori et al. suggested that a reaction between Cu^{1+} and molecular oxygen would result in the formation of the hydrogen peroxide required to fuel the Fenton reaction via a two-step process:[15]

$$2Cu^{1+} + 2O_2 \rightarrow 2Cu^{2+} + 2O_2^- \quad \text{Reaction (4)}$$

$$2O_2^- + 2H^+ \rightarrow H_2O_2 + O_2 \quad \text{Reaction (5)}$$

As a strong oxidizing reagent, peroxide is likely to be highly effective towards virus inactivation.[20] As such, the high efficacy for virus inactivation observed in 90% AP solution could also be a result of the production of such reactive species. Further analysis of both of the mechanisms suggested here will require additional study to determine their contribution to the efficacy of virus inactivation, which is beyond the scope of this paper.

The work presented here informs the design of copper alloys, where understanding the true efficacy by which virus deactivation occurs on these surfaces under realistic conditions is essential. We have demonstrated the importance of performing virus inactivation testing in solutions that closely imitate the natural biological solution of interest, and highlighted the reality that virus inactivation on copper surfaces may be significantly more effective than previously thought. Moreover, differing details of test methods may lead to discrepancies in inactivation time, clouding the identification of superior approaches. Accurate information regarding virus inactivation will facilitate design optimization for a critical balance between desired antiviral function, suppression of undesirable tarnish-forming oxides (to maintain aesthetics), color stability, other properties such as formability and suppression of undesirable passivating oxides (that prevent the continued release of cations necessary for virus inactivation). Future virus deactivation testing will be conducted on novel copper alloys, identified in previous work by co-author Scully,[7–9] based on Cu—Al and Cu—Al—Sn. AM:AP virus deactivation test solutions will be utilized based on the work presented here.

4. Conclusion

The work presented here suggests that virus inactivation testing on copper surfaces is highly sensitive to the test solution used. A five-fold decrease in virus half-life was observed in a solution comprised of 90% AP, relative to a solution made from traditional AM only. The critical functional property in the virus inactivation process is the availability of free copper cations, where a critical concentration must be attained relative to each viral target. We have demonstrated that the AM:AP ratio has an influence on: 1) the thickness and composition of the solid molecular compounds formed on the metallic surface during exposures, and 2) the rate of copper cation release. However, we propose a virus inactivation inhibition mechanism by which AM solution has a chelating effect on soluble Cu cations, such that the amount of available Cu for virus deactivation is below the critical threshold. This theory derives from the observation that virus deactivation is inhibited despite an enhanced cation release-rate when pure copper is exposed to 100% AM solution, and a decreasing oxide thickness measured after exposure to an increasing AM:AP ratio. This work highlights the hypo-activating nature of a virus test solution, relative to AP, that clouds the true efficacy by which anti-viral properties are provided by pure copper. We aim to inform future copper alloy design and optimization by highlighting the importance of testing solutions that closely imitate the natural biological solution of interest.

5. Experimental Section

Virus Inactivation Tests: Thawed Betacoronavirus 1 stock was mixed with the indicated solutions. Then 70 uL of virus-containing solutions were spotted on the plastic or CP copper surface for indicated times. At the indicated times, the same amount of the samples was removed from the surface and added to the 96 well plates with HCT-8 cells in the assay medium. After 72 h of incubation, cells were fixed with 4% paraformaldehyde. Then cells were permeabilized with 0.1% Triton, and stained with anti-Coronavirus nucleoprotein (OC-43) (Millipore), followed by staining with IRDye800CW Goat anti-mouse antibody and Cell Tag 700 Stain (Li-Cor). Intensity of the signal of each well was measured by Odyssey CLx(Li-Cor).

Electrochemical Cyclic Voltammetry and Coulometric Reduction: All electrochemical experiments were conducted in Cu ion-free dearated boric acid buffer (pH 8.4), to maintain stable copper oxides, and utilize a three-electrode cell configuration. The copper specimens were used as the working electrode, a Pt mesh was used as the counter electrode and a saturated calomel electrode (SCE) was used as the reference electrode. Prior to each experiment, CP copper specimens were fully immersed in one of the following solutions: (a) no solution, (b) 100% AM, (b) 100% AP, (c) 80% AP + 20% AM, (d) 90% AP + 10% AM for 20 min. CV scans were conducted at a sweep rate of 10 mV s^{-1} between –0.7 and +0.5 V versus SCE. Three sweeps were conducted in each experiment and data from the third sweep was presented. The charge associated with the oxidation of Cu(0) to Cu(I) was calculated by measuring the area under Peak (1) (Figure 3c) via integration and dividing by the scan rate. CR experiments were conducted by applying a galvanostatic hold of –20 μAcm^{-2} and measuring the resulting potential as a function of time. The thickness (δ) of the copper oxides was calculated from the CR potential data using Faraday's Law:

$$\delta = 10^5 QV / nF \quad (3)$$

where δ is measured in Å, F is Faraday's constant (96485 C equiv^{-1}), n is number of equivalents (equivalents/mole), Q is the charge density

($mC\text{-}cm^{-2}$), V is the molar volume for each oxide, where respective values of 12.4 and 23.9 cm^3mol^{-1} were used for CuO and Cu_2O. The thickness of the CuO layer was calculated using the cathodic charge associated with the first plateau. In order to measure the thickness of the original Cu_2O layer formed during the pre-exposure, extraction of the Cu_2O formed during the experiment, as a result of the reduction of CuO, was necessary. This was done by subtracting the charge associated with the first plateau from the total charge from plateaus (2) and (3), which both relate to Cu_2O.

X-Ray Photoelectron Spectroscopy (XPS): The XPS was acquired with a PHI Versaprobe III XPS (Nanoscale Materials Characterization Facility, University of Virginia) using a monochromatic Al Kα source (1486.6 eV KE, 6.5 mA, 20 kV). The analyzer work function was calibrated to give an Au $4f^{7/2}$ metallic gold peak at a BE of 83.96 eV. Instrument base pressure was 5.70×10^{-6} Pa. Survey spectra and high-resolution spectra were obtained using an analysis area of $\approx 100 \times 1400$ µm and pass energies of 200 and 26eV, respectively.

Spectra were analyzed using KolXPD software (version 1.8.0).[39] Elemental copper and associated metal oxide species were fitted according to curve fitting parameters proposed by Biesinger.[40] For species with multiple peaks, their Gaussian widths were correlated relative to one another according to Biesinger's values. The Gaussian width for a species' lowest binding energy feature was determined through the best fits. Similarly, Lorentzian widths for the Cu 2p core levels were fixed to that found for sputtered pure copper. For the Cu LMM, the Lorentzian widths of each species were defined as a percentage of the Gaussian width, following Biesinger's GL(x) parameters. Peak positions were correlated by fixing peak separations following Biesinger's curve fitting parameters, whilst each species' lowest binding energy peak position was determined from the best fits. Finally, all peak integrated intensities were determined via best spectral fits. This procedure ensured that features with multiple components have a fixed shape that can vary only in total area, total width, and total position. The metal oxide peaks in the O 1s spectra were deconvoluted via the aforementioned process, referencing curve fitting parameters proposed by Biesinger et al.[41]

Pure copper samples were exposed to different test solutions for twenty-minute immersions, followed by a rinse in DI water. Samples were then dried using pure nitrogen gas and mounted onto sample holders using conductive carbon tape, before insertion into the XPS system.

Graphite Furnace Atomic Absorption Spectrometry: Total Cu concentrations were measured in 5 mL of 100% AP and 100% AM solutions that had been exposed to CP copper for 20 min. Each exposure was carried out in triplicate. A calibrated graphite furnace (HGA 900, Perkin-Elmer, Waltham, MA, USA) and an atomic absorption spectrometer (AA2100, Perkin-Elmer) (GFAAS) with a copper cathode lamp were used for measurements. Prior to GFAAS analysis, samples were acid digested using trace metal grade nitric acid (Fisher Chemical, Fair Lawn, NJ, USA) for a final sample concentration of 2% nitric acid by volume.

Materials: CP copper (99.95 wt.%, UNS C11000) sheet used in all experiments was obtained from McMaster Carr. Before all experiments, CP copper was ground with successive grades of abrasive SiC grit paper up to 1200 grit, then rinsed with ethanol. Naturally aerated (quiescent) AP solution was made using the standard given in BS EN 1811:2011, designed for evaluating nickel release from jewelry, in the current study pH adjustment to pH 6.50 ± 0.05 was made with NH_4OH instead of NaOH. The composition is given in Table S1, Supporting Information. A boric-borate buffer electrolyte media was prepared using 0.11 M boric acid (H_3BO_3) and 21 mM sodium tetraborate ($Na_2B_4O_7$) for CR experiments at pH 8.40 ± 0.05); at this pH any pre-formed Cu oxides were chemically stable. HCT-8 and Betacoronavirus 1(OC43, CR-1558) were purchased from ATCC. Betacoronavirus 1 were amplified as described in Yang C-W et al.[42] Briefly, Betacoronavirus 1 was propagated in HCT-8 cells cultured in the Assay medium based on Dulbecco's modified eagle medium (DMEM) and 2% fetal bovine serum (FBS) and Pen/Strep. After a significant cytopathic effect was observed, supernatant of the cell culture was stored at −80 °C. Cell rinsing was done using Phosphate buffered saline (PBS). DMEM AM, PBS, and Pen/Strep were obtained from ThermoFisher Scientific. The composition of DMEM (Table S2, Supporting Information), and PBS (Table S3, Supporting Information) are given in the Supporting Information.

Statistical Analysis: The plots presented in Figure 1 were given in terms of mean values ± standard deviation, where n = 3. For Figure 1a *p*-values between plastic and pure Copper were calculated using two-factor with the ANOVA statistical method with replication, for all time points $p < 0.01$. The *p*-values for pure Copper samples were calculated using one-factor ANOVA and, between 20 and 100 min, $p < 0.01$. For Figure 1b the *p*-value was calculated using one-factor ANOVA, where $p < 0.01 (p = 5.73 \times 10^{-7})$. Statistical analysis was carried out using Microsoft EXCEL software. For all electrochemical methods, experiments were conducted in triplicate and representative data has been presented. Error has been presented using the calculated standard deviation for peak area and oxide thickness calculations for CV and CR experiments, respectively. GFAAS experiments were conducted in triplicate and the mean values and standard deviation have been presented.

Supporting Information

Supporting Information is available from the Wiley Online Library or from the author.

Acknowledgements

This work was partially supported by NSF-Rapid #2040273. The authors gratefully acknowledge the National Science Foundation under NSF #162601 MRI acquisition of an x-ray photoelectron spectrometer for chemical mapping of evolving surfaces: a regional instrument for research and teaching.

Conflict of Interest

The authors declare no conflict of interest.

Data Availability Statement

The data that support the findings of this study are available from the corresponding author upon reasonable request.

Keywords

anti-viral high-touch surfaces, copper, electrochemistry, surface characterization, virus mitigation

Received: February 21, 2022
Revised: April 8, 2022
Published online: May 4, 2022

[1] N. van Doremalen, T. Bushmaker, D. H. Morris, M. G. Holbrook, A. Gamble, B. N. Williamson, A. Tamin, J. L. Harcourt, N. J. Thornburg, S. I. Gerber, J. O. Lloyd-Smith, E. de Wit, V. J. Munster, *N. Engl. J. Med.* **2020**, *382*, 1564.
[2] S. L. Warnes, Z. R. Little, C. W. Keevil, *mBio* **2015**, *6*, e01697.
[3] M. Zambon, *Medicine* **2014**, *42*, 45.
[4] World Health Organization 2020, *Sci. Brief* **2020**, 1.
[5] B. Balasubramaniam, Prateek, S. R. , M. Saraf, P. Kar, S. P. Singh, V. K. Thakur, A. Singh, R. K. Gupta, *ACS Pharmacol. Transl. Sci.* **2021**, *4*, 8.

[6] M. Birkett, L. Dover, C. Cherian Lukose, A. Wasy Zia, M. M. Tambuwala, Á. Serrano-Aroca, *Int. J. Mol. Sci.* **2022**, *23*, 1162.
[7] M. J. Hutchison, P. Zhou, K. Ogle, J. R. Scully, *Electrochim. Acta* **2017**, *241*, 73.
[8] M. J. Hutchison, J. R. Scully, *Electrochim. Acta* **2018**, *283*, 806.
[9] L. Foster, M. Hutchson, J. Scully, *Corrosion* **2015**, *72*, 51.
[10] T. Chang, K. Butina, G. Herting, G. K. Rajarao, A. Richter-Dahlfors, E. Blomberg, I. Odnevall Wallinder, C. Leygraf, *Corros. Sci.* **2021**, *185*, 109433.
[11] D. S. Kharitonov, A. A. Kasach, D. S. Sergievich, A. Wrzesińska, I. Bobowska, K. Darowicki, A. Zielinski, J. Ryl, I. I. Kurilo, *Ultrason. Sonochem.* **2021**, *75*, 105593.
[12] M. Vincent, R. E. Duval, P. Hartemann, M. Engels-Deutsch, *J. Appl. Microbiol.* **2018**, *124*, 1032.
[13] J. O. Noyce, H. Michels, C. W. Keevil, *Appl. Environ. Microbiol.* **2007**, *73*, 2748.
[14] P. Bleichert, C. E. Santo, M. Hanczaruk, H. Meyer, G. Grass, *BioMetals* **2014**, *27*, 1179.
[15] Y. Fujimori, T. Sato, T. Hayata, T. Nagao, M. Nakayama, T. Nakayama, R. Sugamata, K. Suzuki, *Appl. Environ. Microbiol.* **2012**, *78*, 951.
[16] X. Hang, H. Peng, H. Song, Z. Qi, X. Miao, W. Xu, *J. Virol. Methods* **2015**, *222*, 150.
[17] N. Hutasoit, B. Kennedy, S. Hamilton, A. Luttick, R. A. R. Rashid, S. Palanisamy, *Manuf. Lett.* **2020**, *25*, 93.
[18] J. R. Scully, *Corrosion* **2020**, *76*, 523.
[19] J. R. Scully, M. Hutchison, R. J. Santucci, *Corrosion* **2021**, *77*, 370.
[20] C. Bryant, S. A. Wilks, C. W. Keevil, *Cell Cult. Infectivity Assay Microbiol.* **2021**.
[21] J. Robinson, A. Arjunan, A. Baroutaji, M. Martí, A. Tuñón Molina, Á. Serrano-Aroca, A. Pollard, *Rapid Prototyp. J.* **2021**, *27*, 1831.
[22] G. Kear, B. D. Barker, F. C. Walsh, *Corros. Sci.* **2004**, *46*, 109.
[23] M. Pourbaix, J. Burbank, *J. Electrochem. Soc.* **1964**, *111*, 14C.
[24] R. Dyrdak, E. B. Hodcroft, M. Wahlund, R. A. Neher, J. Albert, *J. Clin. Virol.* **2021**, *136*, 104754.
[25] O. Jensen, E. Nielsen, *Acta Derm.-Venereol.* **1979**, *59*, 139.
[26] B02 Committee, *Test Method for Coulometric Reduction of Surface Films on Metallic Test Samples*, ASTM International, West Conshohocken, PA **2019**.
[27] S. K. Chawla, B. I. Rickett, N. Sankarraman, J. H. Payer, *Corros. Sci.* **1992**, *33*, 1617.
[28] M. Lenglet, K. Kartouni, D. Delahaye, *J. Appl. Electrochem.* **1991**, *21*, 697.
[29] R. L. Deutscher, R. Woods, *J. Appl. Electrochem.* **1986**, *16*, 413.
[30] S. Lee, R. W. Staehle, *J. Electrochem. Soc.* **1995**, *142*, 2189.
[31] D. Persson, C. Leygraf, *J. Electrochem. Soc.* **1993**, *140*, 1256.
[32] N. Benzbiria, M. Zertoubi, M. Azzi, *Appl. Surf. Sci. Adv.* **2021**, *4*, 100069.
[33] W. Qafsaoui, C. Blanc, N. Pébère, H. Takenouti, A. Srhiri, G. Mankowski, *Electrochim. Acta* **2002**, *47*, 4339.
[34] B. Ehdaie, C. Krause, J. A. Smith, *Environ. Sci. Technol.* **2014**, *48*, 13901.
[35] X. Ding, H. Xie, Y. J. Kang, *J. Nutr. Biochem.* **2011**, *22*, 301.
[36] A. Rakshit, K. Khatua, V. Shanbhag, P. Comba, A. Datta, *Chem. Sci.* **2018**, *9*, 7916.
[37] *The IUPAC Compendium of Chemical Terminology: The Gold Book* (Ed: V. Gold), International Union Of Pure And Applied Chemistry (IUPAC), Research Triangle Park, NC **2019**.
[38] A. Lubej, T. Koloini, C. Pohar, *Acta Chim. Slov.* **2004**, *51*, 18.
[39] KOLXPD, http://kolxpd.kolibrik.net, **2017**.
[40] M. C. Biesinger, *Surf. Interface Anal.* **2017**, *49*, 1325.
[41] M. C. Biesinger, L. W. M. Lau, A. R. Gerson, R. St. C. Smart, *Appl. Surf. Sci.* **2010**, *257*, 887.
[42] C.-W. Yang, T.-T. Peng, H.-Y. Hsu, Y.-Z. Lee, S.-H. Wu, W.-H. Lin, Y.-Y. Ke, T.-A. Hsu, T.-K. Yeh, W.-Z. Huang, J.-H. Lin, H.-K. Sytwu, C.-T. Chen, S.-J. Lee, *Biomed. J.* **2020**, *43*, 368.